ACS Catalysis

pubs.acs.org/acscatalysis

Research Article

Field Effects at Protruding Defect Sites in Electrocatalysis at Metal Electrodes?

Simeon D. Beinlich,* Nicolas G. Hörmann, and Karsten Reuter

Cite This: *ACS Catal.* 2022, 12, 6143–6148

Read Online

ACCESS | Metrics & More | Article Recommendations | Supporting Information

ABSTRACT: Potential dependencies of adsorption energies at metal electrodes are often interpreted in terms of a dipole-field interaction picture. Classical electrostatics would then suggest particularly strong dependencies at protruding defect sites like steps and kinks due to a local field enhancement. Here, we use first-principles density functional theory calculations that capture the capacitive charging of the electric double layer to analyze these dependencies for prototypical adsorbates at vicinal Pt(111) surfaces in an implicit aqueous electrolyte. This analysis confirms effective dipole-field-type dependencies but rationalizes why they can neither be estimated on the basis of accessible molecular dipoles nor the mere atomic-scale geometry of the adsorption site. The observed magnitude questions mechanistic analyses of surface catalytic reactions made on the basis of the prevalent computational hydrogen electrode approach that is agnostic to these potential-induced adsorption energy variations.

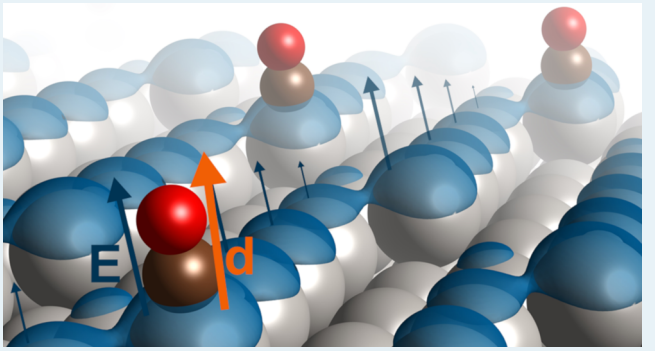

KEYWORDS: *electrochemistry, electrocatalysis, heterogeneous catalysis, adsorption, density functional calculations, dipole-field interactions, electrosorption valency*

INTRODUCTION

The physics of an electrified interface formed by a planar metal electrode and a liquid electrolyte is commonly understood within a plate-capacitor picture. Varying the applied potential away from the point of zero charge (PZC) leads to a charging of the electrode, negative or positive depending on the direction of the potential change. This surface net charge is balanced by the build up of a corresponding counter charge of an equal magnitude and an opposite sign in the electrolyte. The potential drop then occurs over the thus formed narrow electric double layer (DL), leading generally to quite high electric fields at such electrochemical interfaces.[1]

In the widely employed dipole-field interpretation, a dipole moment $\mathbf{d}_\alpha$ of an adsorbate α at the electrode will interact with this electric field $\mathbf{E}$. A leading effect of a variation of the applied potential away from the PZC $\Delta U = U - U_{\mathrm{PZC}}$ on the adsorption energy could therefore simply be a dipole-field type change

$$\Delta E_{\mathrm{ad},\alpha}(\Delta U) = -\mathbf{d}_\alpha \cdot \mathbf{E}(\Delta U) + \cdots \quad (1)$$

with a positive $\Delta E_{\mathrm{ad},\alpha}$ indicating a stronger attachment to the surface. This view seems to be confirmed by recent first-principles calculations that explicitly account for the capacitive charging of the DL away from the PZC.[2−14] Most efficiently but without loss of generality, such calculations are done within an implicit electrolyte model that provides the counter charges when charging up a surface slab within an employed periodic boundary condition supercell.[15] For the low-coverage limit at ideally flat low-index surfaces, where technical differences in determining $\Delta E_{\mathrm{ad},\alpha}(\Delta U)$ in either so-called constant-potential or constant-charge mode vanish,[15,16] the computed potential dependence of adsorption energies even of larger molecules like CO_2 reduction intermediates[2] appears largely understandable in terms of a dipole-field interaction of the type of eq 1. Precisely, this potential dependence, which was not accessible within the earlier and still prevalent so-called computational hydrogen electrode (CHE) approach,[17,18] then rationalizes important conceptual physics like a potential-induced switching of the most stable adsorption site, potential-induced surface reconstructions or lifting of those, or non-Nernstian dependencies of Pourbaix diagrams or cyclic voltammograms.[7,8,19−30]

Even a macroscopically planar electrode is never really completely flat on smaller scales though. The idealized plate-capacitor picture of a laterally evenly distributed net charge and a concomitant homogeneous DL field must therefore be refined by recognizing that under an applied potential, the charge will

Received: February 25, 2022
Revised: April 12, 2022
Published: May 9, 2022

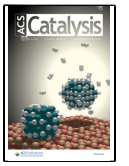

https://doi.org/10.1021/acscatal.2c00997
ACS Catal. 2022, 12, 6143−6148

particularly accumulate in any protrusion of the surface. This will, in turn, lead to a local electric field enhancement at this local curvature. On the mesoscale, such local field effects are known to be relevant, e.g., for dendrite growth, field-enhanced reagent concentration, or tip-enhanced Raman spectroscopy.[31−33]

On even smaller scales, it is intriguing to also view step edge or kink sites as atom-level protrusions between the flat terraces. Already, the undercoordination can generally imply special catalytic properties of such sites. If the dipole-field interaction understanding is extended to these sites, this peculiarity could be further enriched by stronger potential dependencies of adsorption energies due to a local field enhancement.

METHODS

Here, we explore this by fully grand canonical (FGC)[15,19,34] first-principles density functional theory (DFT) calculations for the ideally planar Pt(111) and the kinked Pt(632) and Pt(17 13 12) vicinal surfaces shown in Figure 1. Specifically, we employ

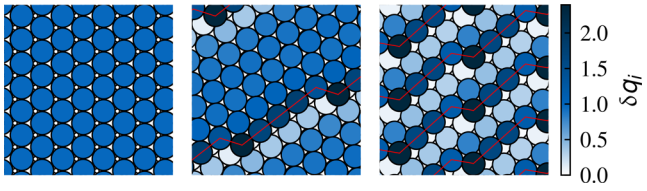

Figure 1. Top view of the Pt(111) (left panel), Pt(17 13 12) (middle panel), and Pt(632) (right panel) surface. The atomic steps with retracting kinks at the latter two vicinal surfaces are marked by thin red lines. The normalized local net charge δq_i on each surface atom i is superimposed as a color code; see text. Note the almost 2.5 times enhancement of δq_i at the most protruding kink atoms, which is independent of the different terrace widths and step lengths of the two vicinal surfaces.

the QuantumEspresso package[35,36] using the PBE DFT exchange−correlation functional[37] in combination with the continuum solvation package Environ,[38] with a comprehensive description of the computational settings provided in the Supporting Information (SI). While the FGC approach with an implicit aqueous electrolyte allows charging the employed surface slab with a total negative (electron excess) or positive (electron deficit) charge Q and a relation $\Delta U = \Delta U(Q)$ to the applied potential can be established, the actual distribution of this total charge over the different surface atoms is an outcome, not an input of the DFT calculation. For different values of Q, we determine these local effective net charges q_i on all surface Pt atoms i by numerically integrating the electronic charge density difference $\Delta\rho_{\mathrm{net}}(Q) = (\rho(Q, \mathbf{r}) - \rho(Q = 0, \mathbf{r}))$ within nonoverlapping atomic volumes V_i found by 3D Voronoi decomposition. The resulting net charges are included in Figure 1 by color-coding the surface atoms. Specifically, we suitably present sign-normalized net charges $\delta q_i = N_{\mathrm{surf}} q_i/Q$ with N_{surf} the number of surface Pt atoms in the employed surface unit cell, as we obtain symmetric results for negative and positive slab charging, as shown in the SI.

RESULTS AND DISCUSSION

For the homogeneous Pt(111) surface, the total surface charge is equally distributed over all surface atoms. For all atoms, $\delta q_i \approx 1$ in the employed normalization, which also demonstrates that almost the entire net charge is located in the outermost atomic layer of the metallic electrode. In contrast to this even distribution, we indeed obtain the expected strong local charge enhancement at the step and kink atoms at the two vicinal surfaces, cf. Figure 1. This enhancement goes up to $\delta q_i = 2.4$ for the most protruding kink atoms, i.e., upon application of a potential, these atoms are charged almost two and a half times as much as the (111) terrace atoms. These relative enhancement values are equally obtained at Pt(632) and Pt(17 13 12), which both exhibit the same (100)-type steps and (111)-type kink retraction, while only differing in the width of the (111) terraces and the step lengths between the kinks, cf. Figure 1. This confirms that the net charge and a concomitant field enhancement is a local property of the specific step and the kink structure. We furthermore find all δq_i to be essentially independent of the amount of absolute charging Q employed, cf. Figure S1 in the SI, which indicates that this relative local field enhancement is independent of the field magnitude. Exploiting the relation $\Delta U = \Delta U(Q)$, we also find the absolute local charges to scale linearly with applied potential, unlike the nonlinear behavior at metallic tips recently reported by others.[31]

With the δq_i independent of field magnitude and a local property of the surface atom type, a dipole-field-like potential dependence of adsorption energies as in eq 1 should be proportional to δq_i. In other words, a stronger variation of $\Delta E_{\mathrm{ad},\alpha}(\Delta U)$ with ΔU would be expected for adsorption sites with a larger net charge and thus a larger local field. In Figure 2,

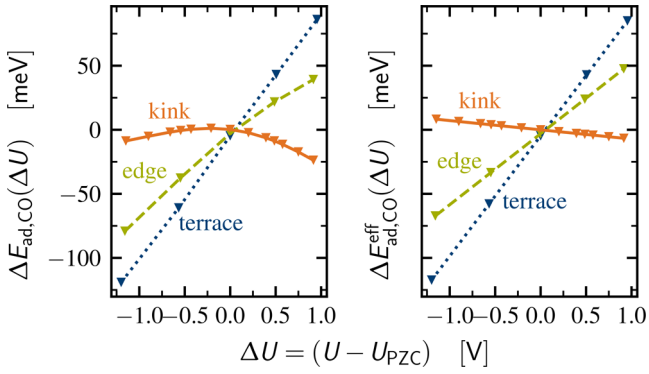

Figure 2. Left panel: FGC-computed potential dependence of the adsorption energy $\Delta E_{\mathrm{ad,CO}}(\Delta U)$ of CO atop terrace sites of Pt(111), as well as atop the kink and step atoms of Pt(632). For the latter step sites, we specifically take the middle atom of the three-atom long steps of Pt(632) that is farthest away from the periodic kink atoms, cf. Figure 1. A local curvature-focused dipole-field picture would suggest a successively stronger potential dependence for terrace, step, and kink sites, which is the opposite of the trend obtained. Right panel: The same as the left panel, but computed with the effective dipole-field expression, as shown in eq 4.

we test this using CO at atop sites as a probe molecule. Intriguingly, the computed adsorption energies at terrace, step, and kink sites show exactly the opposite trend. The weakest potential dependence of $\Delta E_{\mathrm{ad,CO}}(\Delta U)$ is obtained for adsorption atop kink atoms with their high local net charge, whereas the strongest potential dependence is obtained for adsorption atop the low-δq_i terrace atoms.

Notwithstanding this discrepancy, the $\Delta E_{\mathrm{ad,CO}}(\Delta U)$ variations are of the order of magnitude expected for dipole-field interactions. With an atomic-scale width of the electric DL, fields will be of the order of 1 V/Å at an applied potential of 1 V relative to the PZC. Together with the known CO molecular dipole moment of 0.1 Debye, eq 1 yields a potential dependence

https://doi.org/10.1021/acscatal.2c00997
ACS Catal. 2022, 12, 6143−6148

of the adsorption energy of the order of 20 meV/V. This is in the range of the variations observed for step and terrace sites in Figure 2. Furthermore, at least for the latter two sites, $\Delta E_{ad,CO}(\Delta U)$ also shows the overall trend expected from the direction of the molecular dipole moment, i.e., the CO molecule becomes more strongly attached to the electrode with increasing potential.

A straightforward explanation for the discrepancy could thus simply be that the dipole $\mathbf{d}_\alpha$ in eq 1 is not the intrinsic molecular dipole of the adsorbate but an effective one that results after the charge rearrangement upon adsorption.[1,39] Besides small contributions from adsorbate-induced changes of the Pt surface geometry and for a low-coverage, single-adsorption site situation, this surface dipole moment is straightforwardly derived from the work function change $e\Delta\Phi_{PZC,\alpha}$ upon adsorption at the PZC through the Helmholtz equation[39−41]

$$d^{surf}_{z,\alpha} = \epsilon_0 A_{surf} \Delta\Phi_{PZC,\alpha}/N_\alpha \quad (2)$$

with A_{surf} being the area of the surface unit cell and N_α being the number of adsorbates per surface unit cell. As summarized in Table 1, the resulting $\mathbf{d}^{surf}_{CO}$ shows indeed the same ordering as the potential dependencies of the adsorption energies in Figure 2, with the strongest variation of $\Delta E_{ad,CO}(\Delta U)$ for the terrace sites correlating with the largest surface dipole moment. Even the counterintuitive slight decrease of the kink site adsorption energy with increasing potential is nicely rationalized by the direction reversal of the (albeit small) surface dipole moment at this site.

Table 1. Adsorption-Induced Work Function Change at the PZC $\Delta\Phi_{PZC,CO}$ and Surface Dipole Moment d^{surf}_{CO} for the CO Adsorption Atop One Terrace Site at the Pt(111)-(4 × 4) and Atop the Step and Kink Sites at the Pt(632)-(1 × 1) Surface[a]

CO atop	$e\Delta\Phi_{PZC,CO}$ [eV]	d^{surf}_{CO} [Debye]
terrace	−0.10	−0.29
step	−0.11	−0.16
kink	0.01	0.02

[a]Different surface unit cell sizes for the two surfaces lead to the different surface dipole moments for terrace and step sites at comparable work function changes. A positive d^{surf}_{CO} indicates a dipole moment pointing outward from the surface.

Yet, this still does not explain why these dipole-related trends are not affected by the differing charging of the various surface atoms under an applied potential, cf. Figure 1. To this end, it is important to realize that the charge rearrangement upon adsorption will not only affect the dipole moment but also the detailed net charging of the surface atoms upon application of a potential and the concomitant local fields. This can be seen in Figure 3, which shows the δq_i at Pt(632) after adsorption of CO atop the kink sites. Compared to the clean surface, the potential-induced net charging of the kink atoms is dramatically reduced from almost two and a half times as much as the (111) terrace atoms now to δq_i = 0.4. This reduction is almost exclusively restricted to the kink atom to which the CO coordinates. The δq_is of all other surface atoms are barely changed upon adsorption; see the SI for a detailed account. As also summarized in the SI, similarly local reductions of the net charging are obtained at the coordinating Pt atoms upon CO adsorption atop step and terrace sites.

Instead of at the protruding kink atoms, the net charge induced by the applied potential accumulates on the adsorbed CO molecules. This can nicely be seen in the induced net charge density difference shown in Figure 3. Integrated up, we find almost the same amount of net charge on the CO that before resided on the kink atom. From an electrostatic point of view, this is actually quite intuitive if one considers that it is now the CO molecules that by far form the strongest protrusions at the adsorbate-covered surface. It is also consistent with the recent observation in ref 42 that the dominant potential drop of adsorbate-covered surfaces in implicit solvent environments occurs across the vacuum gap between the adsorbate and the implicit model, and to a much lesser extent, only between the metallic surface and the adsorbate. Loosely speaking, the chemisorbed adsorbate thus rather becomes part of the electrode instead of being exposed to the latter's original field.

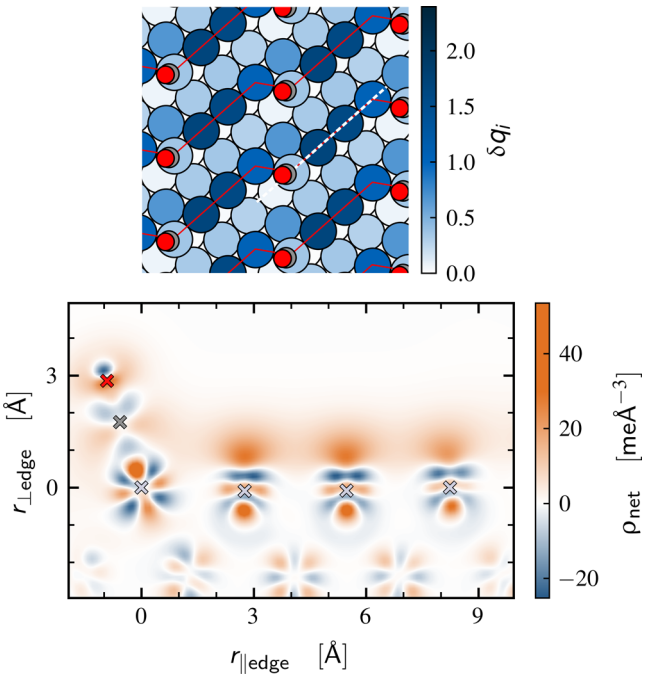

Figure 3. Upper panel: Normalized local net charges δq_i at Pt(632) as in the rightmost panel of Figure 1, but after CO adsorption atop the kink sites (O red spheres, C gray spheres). Note the strong, local reduction of the net charging of the kink atoms in the presence of the adsorbate. Lower panel: Potential-induced net charge density difference $\Delta\rho_{net}(\Delta U(Q)) = (\rho(Q, \mathbf{r}) - \rho(Q = 0, \mathbf{r}))$ at $\Delta U \approx 1$ V within the plane normal to the surface, through the Pt kink atom (light gray cross), the adsorbed CO (gray and red cross), and along the step edge as indicated by the dashed white line in the upper panel. A significant fraction of the net charging ends up on the protruding CO.

The effective local field experienced could thus be more homogeneous than anticipated from the mere atomic-scale geometry of the electrode. In fact, if we simply assume an idealized, completely homogeneous plate-capacitor-type field

$$E^{eff}_z(\Delta U(Q)) = \frac{Q}{\epsilon_o A_{surf}} \quad (3)$$

we exactly arrive at the lowest-order term for the potential-induced variation of the adsorption energy that can be analytically derived for simple solvent models, ideal planar surfaces, and close to the PZC[5,9,10,15,16,34]

$$\Delta E^{eff}_{ad,\alpha}(\Delta U) = -\mathbf{d}^{surf}_\alpha \cdot \mathbf{E}^{eff}(\Delta U(Q)) + \cdots$$
$$= -\Delta\Phi_{PZC,\alpha} Q/N_\alpha + \cdots \quad (4)$$

https://doi.org/10.1021/acscatal.2c00997
ACS Catal. 2022, 12, 6143−6148

Intriguingly, this expression works also surprisingly well for the kinked surface, as shown in Figure 2. The almost quantitative agreement confirms that the observed potential dependencies of $\Delta E_{ad,CO}(\Delta U)$ may indeed be interpreted within a dipole-field picture. As demonstrated in Figure 4, this understanding can

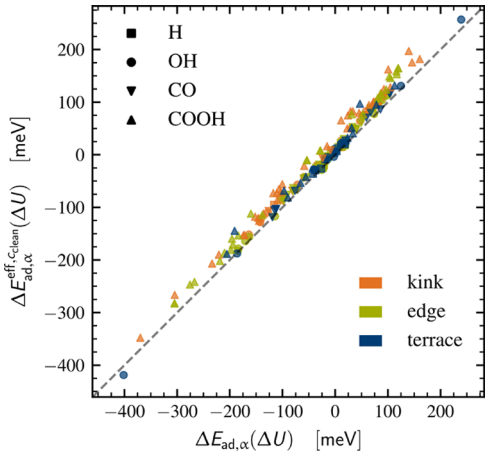

Figure 4. Parity plot of the FGC-computed potential dependence of $\Delta E_{ad,\alpha}(\Delta U)$ with the effective dipole-field dependence of eq 4. Data at ≈±1 V with respect to the PZC for H (■), OH (●), CO (▼), and COOH (▲) are shown in various adsorption modes (top, bridge, threefold) and at terrace (blue), step (green), and kink (red) sites; see text.

also be generalized to other adsorbates and beyond the specific atop adsorption mode. The parity of explicitly FGC-calculated potential-dependent adsorption energies is shown with those computed with the effective dipole-field expression, eq 4, for several prototypical adsorbates (H, OH, CO, COOH) in diverse adsorption modes with varying Pt atom coordination (top, bridge, threefold) and at terrace, step, and kink sites, as explicitly detailed in the SI. Specifically, these data include a manifold of COOH adsorption modes with the terminal H pointing up or down, which each yield different surface dipole moments.

Despite this diversity of adsorption motives, the effective dipole-field expression captures all potential dependencies of $\Delta E_{ad,\alpha}(\Delta U)$ very well. Nevertheless, care has to be exerted not to attribute too much atomistic meaning to this effective picture. This is nicely seen by focusing on the fundamental electrosorption valency $l_\alpha(\Delta U)$, which denotes the number of electrons that flows onto or off the electrode upon adsorption of adsorbate α at applied potential ΔU.[15,34,43] The here-discussed potential dependence of the adsorption energy is derived from the electrical work to charge the double layer with a partial charge $e\delta_\alpha$ to maintain a constant electrode potential,[15,34] and is given by

$$\Delta E_{ad,\alpha}(\Delta U) = -e\delta_\alpha \Delta U \tag{5}$$

where δ_α is related to the electrosorption valency as $e\delta_\alpha = el_\alpha - q_a$, with q_a being the charge of the adsorbate in the solution (e.g., −1e for OH^-). If we now neglect the potential dependence of the electrosorption valency,[34] $e\delta_\alpha(\Delta U) \approx e\delta_\alpha(0) = C_{PZC}A_{surf}\Delta\Phi_{PZC,\alpha}/N_\alpha$, we equally arrive at

$$\Delta E^{eff}_{ad,\alpha}(\Delta U) \approx -C_{PZC}A_{surf}\Delta\Phi_{PZC,\alpha}\Delta U/N_\alpha \tag{6}$$

$$= -\Delta\Phi_{PZC,\alpha}Q/N_\alpha \tag{7}$$

with C_{PZC} being the differential capacitance. This only exploits the general capacitor relation $Q = C_{PZC}A_{surf}\Delta U$, without making any assumptions on the atomic-level homogeneity of the electric field in the DL. Viewing the adsorption energy variations as a consequence of the potential-dependent work required to compensate for the local adsorbate-induced charge flow is thus probably a more powerful physical picture than the commonly employed effective dipole-field interaction interpretation. Note that δ_α is neglected by construction in the CHE approach and the electrosorption valency reduces to the formal charge number of the adsorbate.[34] This is zero for neutral adsorbates like CO, thus leading to potential-invariant adsorption energies.

Equation 6 also provides the starting point for a useful further simplification. If we approximate the differential capacitance with the one of the clean surface at the PZC, $C_{PZC,0}$, the predicted adsorption energy variation

$$\Delta E^{eff}_{ad,\alpha}(\Delta U) \approx -(A_{surf}/N_\alpha)C_{PZC,0}\,\Delta\Phi_{PZC,\alpha}\,\Delta U \tag{8}$$

is almost of the same quality as the one shown in Figure 4 before, cf. Figure S3 in the SI. It is worth noting that this expression is in essence identical to what has been previously used by others.[5,9,10,16,34] This is of high practical value. Table 2 compiles

Table 2. Computed Differential Capacitance at the PZC, $C_{PZC,0}$, in μF cm^{-2}, for a Range of Clean Low-Index Transition Metal Surfaces

	(111)	(001)	(110)
Cu	16.5	16.6	17.5
Rh	16.2	17.3	18.1
Pd	15.5	16.2	16.9
Ag	16.7	17.0	17.2
Ir	14.5	15.4	17.3
Pt	14.3	14.5	15.3
Au	13.4	13.6	14.8

computed $C_{PZC,0}$ for a range of transition metals and surface orientations. Using this data, eq 8 allows to obtain a reliable estimate $\Delta E^{eff}_{ad,\alpha}(\Delta U)$ requiring only quantities that are readily available already within CHE calculations and thus without any need for explicit surface charging, i.e., prominently the adsorbate-induced work function change at the PZC. As such, the influence of these potential dependencies on reaction mechanisms can then swiftly be considered.

CONCLUSIONS

In summary, our analysis thus confirms that potential dependencies of adsorption energies at metal electrodes can largely be interpreted in terms of an effective dipole-field interaction. However, importantly, this concerns the surface dipole that forms upon adsorption, which thus generally precludes simple estimates for the strength of the adsorption energy variation on the basis of accessible molecular dipoles. The charge rearrangement upon specific adsorption also affects the local field experienced by the adsorbate, which precludes estimates merely based on the local atomic-scale electrode geometry. As an important corollary, no particularly strong adsorption energy variation can generally be concluded for protruding defect sites like steps and kinks, contrary to what one intuitively expects from a traditional dipole-field picture.

On the other hand, as demonstrated here, simple estimates can be derived that allow semiquantitative predictions of the potential dependence of the adsorption energy based only on

https://doi.org/10.1021/acscatal.2c00997
ACS Catal. 2022, 12, 6143−6148

knowledge of the adsorbate-induced work function change at the point of zero charge, cf. eq 8. Moreover, as illustrated for several prototypical adsorbates, these dependencies can well reach 300 meV/V, even for adsorbates for which no variation may intuitively have been expected. Changes of this magnitude may well critically affect reaction mechanisms, in particular when it concerns more subtle selectivities. This is of utmost importance, as a dominant part of published first-principles reaction mechanisms in electrocatalysis at metal electrodes has so far been computed without considering these dependencies. It remains to be seen how well the gained insights thus extrapolate to the true working potentials.

■ ASSOCIATED CONTENT

Supporting Information

The Supporting Information is available free of charge at https://pubs.acs.org/doi/10.1021/acscatal.2c00997.

Additional details on DFT, continuum solvation, FGC, effective dipole-field expression, charging of surface atoms, and adsorbate configurations (PDF)

■ AUTHOR INFORMATION

Corresponding Author

Simeon D. Beinlich − *Fritz-Haber-Institut der Max-Planck-Gesellschaft, 14195 Berlin, Germany; Chair for Theoretical Chemistry and Catalysis Research Center, Technische Universität München, 85747 Garching, Germany;* orcid.org/0000-0002-3011-9614; Email: beinlich@fhi.mpg.de

Authors

Nicolas G. Hörmann − *Fritz-Haber-Institut der Max-Planck-Gesellschaft, 14195 Berlin, Germany;* orcid.org/0000-0001-6944-5575

Karsten Reuter − *Fritz-Haber-Institut der Max-Planck-Gesellschaft, 14195 Berlin, Germany;* orcid.org/0000-0001-8473-8659

Complete contact information is available at: https://pubs.acs.org/10.1021/acscatal.2c00997

Funding

Open access funded by Max Planck Society.

Notes

The authors declare no competing financial interest.

■ ACKNOWLEDGMENTS

The authors gratefully acknowledge funding within the German Research Foundation (DFG) project RE1509/33-1 and the DFG CoE e-conversion EXC 2089/1. They gratefully acknowledge the Gauss Centre for Supercomputing e.V. (www.gauss-centre.eu) for providing computing time on the GCS Supercomputer JUWELS at Jülich Supercomputing Centre (JSC).

■ REFERENCES

(1) Schmickler, W.; Santos, E. *Interfacial Electrochemistry*, 2nd ed.; Springer: Berlin, Heidelberg, 2010; pp. 4, 57−58.

(2) Zhang, H.; Goddard, W. A.; Lu, Q.; Cheng, M.-J. The importance of grand-canonical quantum mechanical methods to describe the effect of electrode potential on the stability of intermediates involved in both electrochemical CO2 reduction and hydrogen evolution. *Phys. Chem. Chem. Phys.* **2018**, *20*, 2549−2557.

(3) Bonnet, N.; Dabo, I.; Marzari, N. Chemisorbed Molecules under Potential Bias: Detailed Insights from First-Principles Vibrational Spectroscopies. *Electrochim. Acta* **2014**, *121*, 210−214.

(4) Chen, L. D.; Urushihara, M.; Chan, K.; Nørskov, J. K. Electric Field Effects in Electrochemical CO2 Reduction. *ACS Catal.* **2016**, *6*, 7133−7139.

(5) Clark, E. L.; Ringe, S.; Tang, M.; Walton, A.; Hahn, C.; Jaramillo, T. F.; Chan, K.; Bell, A. T. Influence of Atomic Surface Structure on the Activity of Ag for the Electrochemical Reduction of CO2 to CO. *ACS Catal.* **2019**, *9*, 4006−4014.

(6) Gauthier, J. A.; Dickens, C. F.; Heenen, H. H.; Vijay, S.; Ringe, S.; Chan, K. Unified Approach to Implicit and Explicit Solvent Simulations of Electrochemical Reaction Energetics. *J. Chem. Theory Comput.* **2019**, *15*, 6895−6906.

(7) Hörmann, N. G.; Reuter, K. Thermodynamic Cyclic Voltammograms Based on Ab Initio Calculations: Ag(111) in Halide-Containing Solutions. *J. Chem. Theory Comput.* **2021**, *17*, 1782−1794.

(8) Hörmann, N. G.; Reuter, K. Thermodynamic cyclic voltammograms: peak positions and shapes. *J. Phys.: Condens. Matter* **2021**, *33*, No. 264004.

(9) Kelly, S. R.; Kirk, C.; Chan, K.; Nørskov, J. K. Electric Field Effects in Oxygen Reduction Kinetics: Rationalizing pH Dependence at the Pt(111), Au(111), and Au(100) Electrodes. *J. Phys. Chem. C* **2020**, *124*, 14581−14591.

(10) Lamoureux, P. S.; Singh, A. R.; Chan, K. pH Effects on Hydrogen Evolution and Oxidation over Pt(111): Insights from First-Principles. *ACS Catal.* **2019**, *9*, 6194−6201.

(11) Resasco, J.; Chen, L. D.; Clark, E.; Tsai, C.; Hahn, C.; Jaramillo, T. F.; Chan, K.; Bell, A. T. Promoter Effects of Alkali Metal Cations on the Electrochemical Reduction of Carbon Dioxide. *J. Am. Chem. Soc.* **2017**, *139*, 11277−11287.

(12) Ringe, S.; Clark, E. L.; Resasco, J.; Walton, A.; Seger, B.; Bell, A. T.; Chan, K. Understanding cation effects in electrochemical CO2 reduction. *Energy Environ. Sci.* **2019**, *12*, 3001−3014.

(13) Ringe, S.; Morales-Guio, C. G.; Chen, L. D.; Fields, M.; Jaramillo, T. F.; Hahn, C.; Chan, K. Double layer charging driven carbon dioxide adsorption limits the rate of electrochemical carbon dioxide reduction on Gold. *Nat. Commun.* **2020**, *11*, No. 33.

(14) Vijay, S.; Gauthier, J. A.; Heenen, H. H.; Bukas, V. J.; Kristoffersen, H. H.; Chan, K. Dipole-Field Interactions Determine the CO2 Reduction Activity of 2D Fe-N-C Single-Atom Catalysts. *ACS Catal.* **2020**, *10*, 7826−7835.

(15) Ringe, S.; Hörmann, N. G.; Oberhofer, H.; Reuter, K. Implicit Solvation Methods for Catalysis at Electrified Interfaces *Chem. Rev.* 2021, DOI: 10.1021/acs.chemrev.1c00675.

(16) Gauthier, J. A.; Dickens, C. F.; Ringe, S.; Chan, K. Practical Considerations for Continuum Models Applied to Surface Electrochemistry. *ChemPhysChem* **2019**, *20*, 3074−3080.

(17) Nørskov, J. K.; Rossmeisl, J.; Logadottir, A.; Lindqvist, L.; Kitchin, J. R.; Bligaard, T.; Jónsson, H. Origin of the Overpotential for Oxygen Reduction at a Fuel-Cell Cathode. *J. Phys. Chem. B* **2004**, *108*, 17886−17892.

(18) Rossmeisl, J.; Logadottir, A.; Nørskov, J. K. Electrolysis of water on (oxidized) metal surfaces. *Chem. Phys.* **2005**, *319*, 178−184.

(19) Hörmann, N. G.; Andreussi, O.; Marzari, N. Grand canonical simulations of electrochemical interfaces in implicit solvation models. *J. Chem. Phys.* **2019**, *150*, No. 041730.

(20) Sundararaman, R.; Goddard, W. A., 3rd; Arias, T. A. Grand canonical electronic density-functional theory: Algorithms and applications to electrochemistry. *J. Chem. Phys.* **2017**, *146*, No. 114104.

(21) Mathew, K.; Kolluru, V. S. C.; Mula, S.; Steinmann, S. N.; Hennig, R. G. Implicit self-consistent electrolyte model in plane-wave density-functional theory. *J. Chem. Phys.* **2019**, *151*, No. 234101.

(22) Kim, D. H.; Ringe, S.; Kim, H.; Kim, S.; Kim, B.; Bae, G.; Oh, H.-S.; Jaouen, F.; Kim, W.; Kim, H.; Choi, C. H. Selective electrochemical reduction of nitric oxide to hydroxylamine by atomically dispersed iron catalyst. *Nat. Commun.* **2021**, *12*, No. 1856.

(23) Bonnet, N.; Marzari, N. First-principles prediction of the equilibrium shape of nanoparticles under realistic electrochemical conditions. *Phys. Rev. Lett.* **2013**, *110*, No. 086104.
(24) Weitzner, S. E.; Dabo, I. Voltage-dependent cluster expansion for electrified solid-liquid interfaces: Application to the electrochemical deposition of transition metals. *Phys. Rev. B* **2017**, *96*, No. 205134.
(25) Cheng, T.; Wang, L.; Merinov, B. V.; Goddard, W. A. Explanation of Dramatic pH-Dependence of Hydrogen Binding on Noble Metal Electrode: Greatly Weakened Water Adsorption at High pH. *J. Am. Chem. Soc.* **2018**, *140*, 7787−7790.
(26) Huang, J.; Hörmann, N.; Oveisi, E.; Loiudice, A.; De Gregorio, G. L.; Andreussi, O.; Marzari, N.; Buonsanti, R. Potential-induced nanoclustering of metallic catalysts during electrochemical CO2 reduction. *Nat. Commun.* **2018**, *9*, No. 3117.
(27) Karmodak, N.; Andreussi, O. Catalytic Activity and Stability of Two-Dimensional Materials for the Hydrogen Evolution Reaction. *ACS Energy Lett.* **2020**, *5*, 885−891.
(28) Kopač Lautar, A.; Bitenc, J.; Dominko, R.; Filhol, J.-S. Building Ab Initio Interface Pourbaix diagrams to Investigate Electrolyte Stability in the Electrochemical Double Layer: Application to Magnesium Batteries. *ACS Appl. Mater. Interfaces* **2021**, *13*, 8263−8273.
(29) Jinnouchi, R.; Kodama, K.; Nagoya, A.; Morimoto, Y. Simulated Volcano Plot of Oxygen Reduction Reaction on Stepped Pt Surfaces. *Electrochim. Acta* **2017**, *230*, 470−478.
(30) Gauthier, J. A.; Ringe, S.; Dickens, C. F.; Garza, A. J.; Bell, A. T.; Head-Gordon, M.; Nørskov, J. K.; Chan, K. Challenges in Modeling Electrochemical Reaction Energetics with Polarizable Continuum Models. *ACS Catal.* **2019**, *9*, 920−931.
(31) Santos, E.; Schmickler, W. The Crucial Role of Local Excess Charges in Dendrite Growth on Lithium Electrodes. *Angew. Chem., Int. Ed.* **2021**, *60*, 5876−5881.
(32) Liu, M.; Pang, Y.; Zhang, B.; De Luna, P.; Voznyy, O.; Xu, J.; Zheng, X.; Dinh, C. T.; Fan, F.; Cao, C.; de Arquer, F. P. G.; Safaei, T. S.; Mepham, A.; Klinkova, A.; Kumacheva, E.; Filleter, T.; Sinton, D.; Kelley, S. O.; Sargent, E. H. Enhanced electrocatalytic CO2 reduction via field-induced reagent concentration. *Nature* **2016**, *537*, 382−386.
(33) Sonntag, M. D.; Pozzi, E. A.; Jiang, N.; Hersam, M. C.; Duyne, R. P. V. Recent Advances in Tip-Enhanced Raman Spectroscopy. *J. Phys. Chem. Lett.* **2014**, *5*, 3125−3130.
(34) Hörmann, N. G.; Marzari, N.; Reuter, K. Electrosorption at metal surfaces from first principles. *npj Comput. Mater.* **2020**, *6*, No. 136.
(35) Giannozzi, P.; Baroni, S.; Bonini, N.; Calandra, M.; Car, R.; Cavazzoni, C.; Ceresoli, D.; Chiarotti, G. L.; Cococcioni, M.; Dabo, I.; Dal Corso, A.; de Gironcoli, S.; Fabris, S.; Fratesi, G.; Gebauer, R.; Gerstmann, U.; Gougoussis, C.; Kokalj, A.; Lazzeri, M.; Martin-Samos, L.; Marzari, N.; Mauri, F.; Mazzarello, R.; Paolini, S.; Pasquarello, A.; Paulatto, L.; Sbraccia, C.; Scandolo, S.; Sclauzero, G.; Seitsonen, A. P.; Smogunov, A.; Umari, P.; Wentzcovitch, R. M. QUANTUM ESPRESSO: a modular and open-source software project for quantum simulations of materials. *J. Phys. Condens. Matter* **2009**, *21*, No. 395502.
(36) Giannozzi, P.; Andreussi, O.; Brumme, T.; Bunau, O.; Buongiorno Nardelli, M.; Calandra, M.; Car, R.; Cavazzoni, C.; Ceresoli, D.; Cococcioni, M.; Colonna, N.; Carnimeo, I.; Dal Corso, A.; de Gironcoli, S.; Delugas, P.; DiStasio, R. A.; Ferretti, A.; Floris, A.; Fratesi, G.; Fugallo, G.; Gebauer, R.; Gerstmann, U.; Giustino, F.; Gorni, T.; Jia, J.; Kawamura, M.; Ko, H.-Y.; Kokalj, A.; Küçükbenli, E.; Lazzeri, M.; Marsili, M.; Marzari, N.; Mauri, F.; Nguyen, N. L.; Nguyen, H.-V.; Otero-de-la Roza, A.; Paulatto, L.; Poncé, S.; Rocca, D.; Sabatini, R.; Santra, B.; Schlipf, M.; Seitsonen, A. P.; Smogunov, A.; Timrov, I.; Thonhauser, T.; Umari, P.; Vast, N.; Wu, X.; Baroni, S. Advanced capabilities for materials modelling with Quantum ESPRESSO. *J. Phys. Condens. Matter* **2017**, *29*, No. 465901.
(37) Perdew, J. P.; Burke, K.; Ernzerhof, M. Generalized Gradient Approximation Made Simple. *Phys. Rev. Lett.* **1996**, *77*, 3865−3868.
(38) Andreussi, O.; Dabo, I.; Marzari, N. Revised self-consistent continuum solvation in electronic-structure calculations. *J. Chem. Phys.* **2012**, *136*, No. 064102.
(39) Gossenberger, F.; Roman, T.; Forster-Tonigold, K.; Groß, A. Change of the work function of platinum electrodes induced by halide adsorption. *Beilstein J. Nanotechnol.* **2014**, *5*, 152−161.
(40) Todorova, M.; Reuter, K.; Scheffler, M. Oxygen Overlayers on Pd(111) Studied by Density Functional Theory. *J. Phys. Chem. B* **2004**, *108*, 14477−14483.
(41) Li, W.-X.; Stampfl, C.; Scheffler, M. Oxygen adsorption on Ag(111): A density-functional theory investigation. *Phys. Rev. B* **2002**, *65*, No. 075407.
(42) Sundararaman, R.; Figueiredo, M. C.; Koper, M. T. M.; Schwarz, K. A. Electrochemical Capacitance of CO-Terminated Pt(111) Dominated by the CO-Solvent Gap. *J. Phys. Chem. Lett.* **2017**, *8*, 5344−5348.
(43) Schmickler, W. The surface dipole moment of species adsorbed from a solution. *J. Electroanal. Chem. Interfacial Electrochem.* **1988**, *249*, 25−33.

https://doi.org/10.1021/acscatal.2c00997
ACS Catal. 2022, 12, 6143−6148